NASA Technical Memorandum 106135

Calculations of Combustion Response Profiles and Oscillations

Richard J. Priem
Priem Consultants Inc.
Cleveland, Ohio

and

Kevin J. Breisacher
Lewis Research Center
Cleveland, Ohio

Prepared for the
First International Symposium on Liquid Rocket Combustion Instability
sponsored by Pennsylvania State University
University Park, Pennsylvania, January 18–20, 1993

NASA

CALCULATIONS OF COMBUSTION RESPONSE PROFILES AND OSCILLATIONS

Richard J. Priem
Priem Consultants Inc.
Cleveland, Ohio

Kevin J. Breisacher
NASA Lewis Research Center
Cleveland, Ohio

ABSTRACT

The theory and procedures for determining the characteristics of pressure oscillations in rocket engines with prescribed burning rate oscillations are presented. Pressure and velocity oscillations calculated using this procedure are presented for the SSME to show the influence of baffles and absorbers on the burning rate oscillations required to achieve neutral stability. Results of calculations to determine local combustion responses using detailed physical models for injection, atomization, and vaporization with gas phase oscillations in baffled and unbaffled SSME combustors are presented. The contributions of the various physical phenomena occurring in a combustor to oscillations in combustion response have been determined.

INTRODUCTION

Any review of liquid rocket combustion instability model development in the United States prior to 1972, inevitably leads to NASA SP-194 [1]. This publication is a compendium of the combustion instability modeling efforts by industrial, academic, and government teams from across the nation. Their efforts were aided by the considerable financial support these groups received during the 1960's due to the perceived threat of combustion instabilities to achieving national space goals. The work of these groups also benefitted from the considerable experimental studies of combustion instability phenomenon including liquid rocket combustion tests.

After 1972, financial support for combustion instability research was drastically reduced and very little effort was devoted to the subject. In the interim, major advances were made in the computational capability of computers and in numerical solution techniques for non-linear partial differential equations. This increase in capability has permitted investigators to make calculations that were only dreams in the early 1970's. Increased computational capabilities also allowed the development of new quantitative spray measurement techniques.

Atomization was shown to be an important mechanism in combustion instability in numerous experimental studies. Experimental studies [2-4] clearly illustrate the drastic spatial and temporal changes that occur in the atomization process during an instability. To this day, the quantification and simulation of the atomization process remains a considerable challenge to the understanding and

control of combustion instability in liquid rocket engines.

STATUS AS OF 1972

The majority of the modeling efforts prior to 1972 used linear or nonlinear acoustics but very cursory combustion models. Modeling efforts representative of this era were made by Crocco and his colleagues at Princeton [5-8], Culick [9], and Priem [10]. These models were used to gain an understanding of instabilities and guide engine design changes intended to achieve stability. In general, the differences between the chamber response obtained with linear and nonlinear acoustic models were small[6,7]. Some models for chamber acoustics included the separate effects of baffles (radial baffles or hub baffles but not combinations of hub and radial baffles) and acoustic absorbers but not the combined effects of baffles and absorbers. With these models of chamber acoustics, designers had a greater ability to predict the need for and proper design of acoustic absorbers.

The combustion models used in the frequency domain codes related the local instantaneous combustion rate to the local pressure using two constants (i.e. n and tau or a complex combustion response). Reardon[11] did correlate time lag parameters with engine design and operating parameters. These correlations were also used as a guide to obtaining stable engine configurations. Individual combustion processes such as injection, atomization, and vaporization were too computationally intensive to model and in the case of atomization detailed models were not available. Movies of the combustion zone in experimental combustors[2] have shown the highly nonlinear nature of the combustion process during an instability. During a full-blown instability, it almost appeared as if a detonation wave was traversing the combustion zone. It is not suprising that the simple two constant combustion models could not provide a detailed understanding of instability or a quantitative evaluation of the influence of design and operating changes on stability.

Numerical studies[12,13] were conducted to examine the response of individual combustion processes (injection, atomization, vaporization, and chemical reaction) to idealized chamber acoustic waves. These acoustic waves corresponded to the resonant frequency of cylindrical chambers with no stability aids, axial velocity profiles, and ideal nozzles. The studies demonstrated that all of the individual processes were capable of driving an instability. The result of these studies were correlated to provide n-tau combustion models. None of the frequency domain models of this era attempted a comprehensive model that tracked the propellant from the injector until it was completely burned.

Simple one and two dimensional time domain combustion instability models[14-16] were developed prior to 1972. Although these codes typically modeled injection, a mechanistic treatment of atomization was omitted. The combustion rate was usually modelled as an empirical function of pressure. None of these early time domain codes had a "complete" combustion model. The codes were able to demonstrate the existence of a minimum disturbance amplitude necessary to initiate an instability. The wave characteristics calculated with these codes were similar to those observed from dynamic stability tests. These codes had considerable problems with numerical stability, particularly the two dimensional codes.

DESIGN TOOLS FOR THE 1990's

The goal of current stability code development efforts is to produce a collection of analysis tools to allow a designer to assess the stability margin of candidate combustor designs. This collection of codes may include fast, acoustic n-tau codes for preliminary design screening. Fourier time expansion and simple time domain codes could be utilized for stability margin evaluation and stability aid design for candidate combustor designs. Rigorous time domain codes could be used for final design evaluation. The features of these codes are summarized in Table I. and are discussed below.

Any analysis of combustion instability in rocket engines is only as accurate as the specification of the boundary conditions for the problem. Unfortunately, the boundary conditions for stability analyses in liquid rocket engines are highly nonlinear and not very well understood. The rate and location at which injected propellant is atomized and the resulting size and velocity of the droplets is crucial input to any instability analysis. The subsequent behavior of the propellant as it burns or undergoes further breakups is critically linked to the atomization boundary condition. This boundary condition is also part of a highly nonlinear feedback loop in which the combustor gas field influences atomization and atomization influences burning and the combustor velocity profile. Accurately modeling this phenomena is the paramount challenge of rocket combustor modelling.

Typically, a shear coaxial element is modeled using correlations developed from cold flow tests. These correlations provide a relationship between global parameters (gas velocity, liquid flowrate, jet diameter, etc.) and drop size or atomization rate. Unfortunately in many models, these global correlations have been applied in a subgrid fashion. The overall significance of droplet coalescence and secondary breakup phenomena has not been demonstrated. Secondary breakup is typically modelled using a spring mass oscillator analogy or linear surface wave growth rates even though the majority of experimental evidence suggests a violent stripping phenomena. One can imagine the difficulty in trying to model the drop size produced by an impinging element subject to a high amplitude transverse wave.

The biggest advantage of time domain codes is that they can provide a complete time history of any parameter of interest. These time histories allow for a direct comparison with engine test results. Physical submodel development and code validation is also facilitated by use of these time histories. Interaction between different modes of oscillations is handled automatically, within the filtering limits of the finite difference method.

Updating of one and two dimensional time domain codes to take advantage of the increase in knowledge of the stability characteristics of various finite differencing techniques is underway. However, most instabilities due to injector design or the wave dynamics are inherently three dimensional. A fully three dimensional simulation of the SSME (manifolds, baffles, absorbers, and 600 injection elements) is beyond current computational capabilities, even if atomization could be modeled adequately. Computational time remains a major drawback of the time domain approach.

TABLE I

THREE APPROACHES TO INSTABILITITY MODELING

Acoustics-Simple Combustion	Time Domain CFD	Fourier Time Expansion
FEATURES:		
-linear amplitude or mode series expansion	-time history all parameters.	-Fourier expansion in time
-continuity and momentum conserved	-continuity, momentum, and energy conserved	-continuity and momentum conserved
-simple combustion two parameters	-mechanistic combustion model	-mechanistic combustion model
-stability aids modeled	-stability aids modeled	-stability aids modeled
ADVANTAGES:		
-identifies problem modes	-includes all nonlinear effects	-determines margin
-results obtained quickly	-direct comparison to stability tests	-simulates resulting oscillation
DISADVANTAGES:		
-poor modeling of combustion	-computationally intense	-no real time history generated
-difficult to determine instability source	-different runs for each disturbance level,type	-no interaction between modes

The Fourier time expansion (FTE) approach is something of a hybrid between the time domain, CFD approach and the analytical, acoustic modeling approach. In the FTE approach, the thermodynamic variables and velocity components are expanded in a Fourier time series and substituted in the appropriate conservation equations. The resulting equations are differenced and solved numerically to determine the gas phase oscillations. All the basic combustion processes are modeled as they would be in a time domain approach and then converted into complex responses for use with the FTE approach. Solutions are obtained at different oscillation amplitude levels for the complex frequency (observed frequency and decay rate). The oscillation amplitude at which the decay rate changes from negative to positive is the minimum disturbance amplitude required to excite that mode of instability. The oscillation amplitude at which the decay rate changes back from positive to negative is the equilibrium or "limit cycle" amplitude of the instability. A disadvantage of the FTE approach is that it does not permit having oscillations present with different basic frequencies, i.e. chug and a high frequency oscillation or two transverse modes with different frequencies that beat. Another disadvantage is that no time history of flow parameters is calculated directly for comparison with experiments.

THEORY FOR THE FOURIER TIME EXPANSION

In the remaining portion of the paper, the theory for the Fourier time expansion (FTE) model will be discussed and calculations made using the method will be presented for an SSME combustor. The results of the FTE approach was developed for incorporation into HICCIP (High Frequency Injection Coupled Combustion Instability Program)[24-26]. The code described in ref. 24 was restricted to using wave characteristics derived from a pseudo 3D theory. The code assumed uniform combustion response at all radial and tangential positions for a given axial position. Also, the wave model used could not account for the presence of baffles and discrete absorbers. Therefore, a 3D model for the chamber gas oscillations was required for HICCIP to predict the characteristics in a typical rocket engine.[25,26]

The gas phase oscillations calculated with the 3D FTE approach are used to determine burning rate oscillations throughout the combustor. This is an "open loop" calculation where burning rate oscillations are assumed and used to calculate gas phase oscillations. The gas phase oscillations are then used to calculate burning rate oscillations. If the final calculated burning rate oscillations agreed with the assumed burning rate, a consistent, complete solution would have been obtained. To close the loop, and obtain the complete solution would require iterating the procedure described above. Work is continuing toward completing the "closed loop" model.

The basic conservation equations used to define flow in a cylindrical chamber are:

CONSERVATION OF MASS:

$$\frac{\partial \rho}{\partial t} + \nabla \cdot (\rho \boldsymbol{V}) = W$$

CONSERVATION OF MOMENTUM:

$$\frac{\partial (\rho \boldsymbol{V})}{\partial t} + \nabla \cdot \rho \boldsymbol{V}\boldsymbol{V} + g \nabla P = W \boldsymbol{V}_{liq}$$

ADIABATIC IDEAL GAS:

$$\frac{P}{P_o} = \left(\frac{\rho}{\rho_o}\right)^{\gamma}$$

Where:

ρ	gas density, lb/in^3
V	gas velocity vector, in/s
P	pressure, lb/in^2
t	time, s
W	local burning rate, lb/in^3 s
V_{liq}	velocity of the injected liquid, in/s
g	conversion constant, lbm in/lbf s^2 (386.4)
∇	space derivative, in^{-1}

It is assumed that viscous and gravitational forces are negligible. To simplify the analysis, it is further assumed that the radial and azimuthal steady or average flows are minimal and are therefore zero. This avoids requiring a 3D steady state or time average solution to determine radial and azimuthal flow and pressure profiles.

As in HICCIP, all the variables (P, ρ, V_z, V_r, V_a, W) are expanded in a Fourier time series as given by:

$$F=F_o+F_1e^{i\omega t}+F_2e^{2i\omega t}+\ldots.+F_ne^{ni\omega t}+\ldots$$

Where: F_o is the time averaged variable
F_n is a variable in all three dimensions

Consistent with the above assumptions:
ρ_o & P_o vary only in the axial direction
V_{ro} & V_{ao} are zero (no radial or tangential average flow)
V_{zo} & W_o are variable in all three space dimensions.

All of the equations are nonlinear. In the remaining portion of this paper, only the terms through F_1 are used as these terms are not influenced by the F_2, and higher n terms (since low frequency cross products produce higher harmonic frequencies). After determining the F_1 values the equations could again be solved using the known F_o and F_1 values to find the F_2 values. This process could be continued to determine as many F_n values as required to "completely and rigorously" define the oscillations. Solutions for the F_1 values will define the complex frequency of the oscillations (both the observed frequency and the damping or growth rate).

Substituting the Fourier time series into the conservation equations and retaining only the terms containing "F_o and F_1" yields the following set of equations:
CONTINUITY:

$$i\omega\rho_1+\frac{1}{r}\frac{\partial(r\rho_oV_{r_1})}{\partial r}+\frac{1}{r}\frac{\partial(\rho_oV_{a_1})}{\partial\theta}+\frac{\partial(\rho_oV_{z_1})}{\partial z}+\frac{\partial(\rho_1V_{z_o})}{\partial z}=W_1 \qquad Eq.1$$

AXIAL MOMENTUM:

$$i\omega\rho_oV_{z_1}+i\omega\rho_1V_{z_o}+2\frac{\partial(\rho_oV_{z_o}V_{z_1})}{\partial z}+\frac{\partial(\rho_1V_{z_o}V_{z_o})}{\partial z}+\frac{1}{r}\frac{\partial(r\rho_oV_{r_1}V_{z_o})}{\partial r}+\frac{1}{r}\frac{\partial(\rho_oV_{a_1}V_{z_o})}{\partial\theta}+\gamma\frac{P_o}{\rho_o}\frac{\partial\rho_1}{\partial z}=W_1V_{liq} \qquad Eq.2$$

RADIAL MOMENTUM:

$$i\omega\rho_oV_{r_1}+\frac{\partial(\rho_oV_{z_o}V_{r_1})}{\partial z}+\gamma\frac{P_o}{\rho_o}\frac{\partial\rho_1}{\partial r}=0 \qquad Eq.3$$

AZIMUTHAL MOMENTUM:

$$i\omega\rho_o V_{a_1} + \frac{\partial(\rho_o V_{z_o} V_{a_1})}{\partial z} + \gamma \frac{P_o}{r\rho_o} \frac{\partial P_1}{\partial \theta} = 0 \qquad Eq.4$$

ADIABATIC IDEAL GAS:

$$P_1 = \gamma \frac{P_o}{\rho_o} \rho_1 \qquad Eq.5$$

The boundary conditions for the combustor are:

Chamber Wall

$$V_{r_1} = \gamma \; RspWall \; P_1$$

where "RspWall" is zero for hard walls and is an input value for wall absorbers (RspWall is ratio of the radial velocity to local pressure).

Center of Chamber (r = 0)

All radial fluxes are zero as the area is zero.

Injector Face

$$V_{z_1} = \gamma \; RspInj \; p_1$$

where "RspInj" is zero for a solid injector face and is input for absorbers on the injector face.

End of Combustion Chamber

$$V_{z_1} = \gamma \; RspNoz \; \rho_1$$

where "RspNoz" is the nozzle response obtained from another program, theory etc. as desired. For this paper it is assumed to be zero (short distributed ideal nozzles).

Baffle surfaces

Radial Baffle	$V_{a1} = 0$	Baffle is at an azimuthal momentum cell face.
Hub Baffle	$V_{r1} = 0$	Baffle is at a radial momentum cell face.

Equations 1 - 4 result in a very sparse matrix when using finite difference equations as illustrated above. Using upwind differencing for fluxes due to steady flow the number of terms in each equation are:

continuity	- 8 terms
axial momentum	- 13 terms
radial momentum	- 4 terms
azimuthal momentum	- 4 terms.

The total number of equations and variables to be solved is determined by the number of cells used in each of the three dimensions as given by:

equations = variables = 4 * Ni * Nj * Nk

Where: Ni number of radial cells
Nj number of azimuthal cells
Nk number of axial cells.

As an example, for Ni=10, Nj=12, and Nk=20, which adequately defines an unbaffled chamber with the fundamental transverse mode there are 12,000 equations with complex variables. Each equation has an average of 7 unknowns. The "W" source term is specified for each cell and is determined using burning models as in HICCIP.

One dimensional or coarse two dimensional solutions can be obtained with a banded Gaussian elimination procedure. For problems with larger grids, the resulting sparse matrix equations are solved using a conjugate gradient algorithm modified for complex variables. Since the matrix is neither symmetric nor positive definite, a quadratic form of the error is minimized. This quadratic form effectively has the square of the condition number of the original matrix. As a result, it is necessary to use double precision on machines with 32 bit word sizes. The current algorithm does not incorporate preconditioning. Crude attempts to implement a "multigrid" solution procedure did not reduce computation time.

1D and 2D MODEL

It is also possible to model the oscillations as 1D or 2D phenomena. This is accomplished by assuming that the oscillations in the radial and/or azimuthal directions can be specified by an analytic wave equation solution in the desired direction. With this assumption, the conservation equations in that direction are not necessarily satisfied. The wave equation is:

$$\Phi = f(z)\, e^{i\omega t} e^{in\theta} J_r(mr)$$

and the variables are determined by:

$$p_1 = C\frac{\partial \Phi}{\partial t}$$

$$V_{z_1} = C\frac{\partial \Phi}{\partial z}$$

$$V_{r_1} = C\frac{1}{r}\frac{\partial \Phi}{\partial r}$$

$$V_{\theta_1} = C\frac{\partial \Phi}{\partial \theta}$$

For one cell, in the radial direction the radial derivatives in equations 1 to 5 are given as follows:

$$\frac{1}{r}\frac{\partial}{\partial r}(r\rho_o V_{r_1}) = \frac{\rho_o}{r}\left[\frac{\partial^2}{\partial r^2}(rJ_n(mr))/\frac{\partial}{\partial r}(J_n(mr))\right]V_{r_1}$$

$$\frac{1}{r}\frac{\partial}{\partial r}(r\rho_o V_{z_o} V_{r_1}) = \frac{\rho_o V_{z_o}}{r}\left[\frac{\partial^2}{\partial r^2}(rJ_n(mr)/\frac{\partial}{\partial r}J_n(mr)\right]V_{r_1}$$

$$\gamma\frac{P_o}{\rho_o}\frac{\partial \rho_1}{\partial r} = \frac{\gamma P_o}{\rho_o}\left[\frac{\partial}{\partial r}(rJ_n(mr))/J_n(mr)\right]\rho_1$$

where the Bessel derivative terms are determined from Bessel function tables (at a radius equal to half the chamber radius) for different Bessel Function indices "m and n" which describe the mode in the radial direction and the tangential mode (n). The calculations then correspond to a very thin annular ring at half the distance to the chamber wall.

Similarly for only one cell in the azimuthal direction the azimuthal derivative in equations 1 to 5 are given as follows:

$$\frac{1}{r}\frac{\partial \rho_o V_{\theta_1}}{\partial \theta} = i\frac{n}{r}V_{\theta_1}$$

$$\frac{1}{r}\frac{\partial(\rho_o V_{z_o} V_{\theta_1})}{\partial \theta} = \frac{\rho_o V_{z_o}}{r} inV_{\theta_1}$$

$$\frac{1}{r}\frac{\partial(\rho_o \rho_1)}{\partial \theta} = \frac{\gamma \rho_o}{r} in\rho_1$$

where n specifies the number of modes in the azimuthal direction. The calculations then correspond to a very thin "pie" section cut out of the chamber.

EXERCISING THE MODEL ON THE SSME

To demonstrate the capability of the Fourier time expansion (FTE) approach, calculations were made for the SSME at nominal operating conditions with and without baffles and absorbers for different oscillation modes. The configuration used to represent the SSME is presented below:

SSME CONFIGURATION

Chamber Diameter	17.74	in.
Cylindrical Length	15.079	in.
Hub Baffle Length	2.0	in.
Hub Baffle Diameter	8.87	in.
Radial Baffles	5	Blades
Radial Baffle Length	2.0	in.
Chamber Pressure	2844	psia
Oxidizer Flow	834.0	lbs/s
Fuel Flow	225.3	lbs/s
Absorber Wall Gap	0.36	in.
Absorber Tuned Freq	3T	Mode
Speed of Sound	5183	ft/s

SSME GAS PHASE OSCILLATIONS

A time averaged combustion profile was used similar to that obtained with a vaporization limited model (50% combustion completed 2.3 inches from the injector, 90 % in 7.5 inches, and 99 % completion within the chamber). The time averaged combustion profile remained constant. This is not a realistic assumption as the gas oscillations do influence the time averaged burning rate. The influence of these oscillations will be evaluated when the FTE approach is combined with the combustion models in HICCIP.

The definition for combustion response is:

$$\text{CombRsp} = \frac{W_1 / W_o}{P_1 / P_o}$$

where:

- W_1 is the perturbation in burning rate, lb/(s in^3)
- W_o is the local average burning rate, lb/(s in^3)
- P_1 is the perturbation in pressure, psi
- P_o is the local average pressure, psi

The combustion response is a vector in the complex plane. The real portion of the combustion response is the magnitude of the nondimensional burning rate oscillation that is in phase with the pressure. The imaginary portion of the combustion response indicates the phasing of combustion relative to pressure. A positive imaginary response indicates that the combustion is leading the time dependent pressure, a negative response indicates combustion is lagging.

Burning rate oscillations were obtained by using a combustion response that did not vary spatially. The simplifications of the burning process, while not rigorous, allow a demonstration of the FTE approach and indicate how some of the combustor design variables influence stability in the SSME.

The combustion response needed to drive various waves in the SSME were calculated iteratively. For a given frequency, a combustion response was assumed and a burning rate oscillation was approximated using an analytical acoustic wave solution. This initial guess at the burning rate oscillation was used to determine oscillating pressure and velocity profiles in the combustor. With the calculated pressure profile and assumed burning rate oscillations, a mass averaged combustion response was calculated. The mass averaged combustion response was then used to calculate a new burning rate oscillation. This process was repeated until the difference in the burning rate was less than 0.003 between successive calculations.

With the assumptions and procedure outlined above, a combustion response for any frequency can be determined. The combustion response was calculated (using a grid size of 4 radial, 10 azimuthal, and 8 axial cells) for the 1T mode and the results are shown in Fig 1. The complex combustion response is plotted as a function of frequency between 1860 and 2060 Hz. Three curves are shown in Fig. 1 corresponding to damping rates of +628 s^{-1}, 0 s^{-1}, -628 s^{-1}. As the frequency is increased, the combustion response changes from combustion lagging pressure to leading pressure and crosses the in phase (1.39 real and zero imaginary) plane at 1960 Hz with neutral damping. Normally, this is considered the "natural frequency" for the 1T mode in this engine. However, depending on the combustion response, oscillations in the engine can occur at other frequencies as shown in Fig 1. Larger combustion responses make the engine unstable, lower values result in a stable engine. Negative imaginary response lowers the tuned frequency from the natural and positive imaginary responses increase the tuned frequency. Similar plots can be obtained for all the modes possible in the chamber. The mode type is determined by the initial assumption for the pressure profile or burning rate oscillations in the chamber.

To illustrate how the FTE approach can be used to determine the influence of design parameters on stability and stability modes, calculations were made to determine the frequency and combustion response for "neutral stability at the natural frequency", i.e. where the combustion response has no imaginary value and the oscillations have zero growth or decay rate. The results of these calculations for different stability aid configurations and modes are presented in Table II.

TABLE II

NEUTRAL STABILITY CONDITIONS FOR SSME

Mode	Frequency	Response
UNBAFFLED AND NO ABSORBER (Grid of 8*1*16)		
1 L	1966	1.69
1 T	2057	1.69
2 T	3407	1.65
3 T	4686	1.64
UNBAFFLED AND ORIGINAL SSME ABSORBER (Grid of 8*1*16)		
1 L	1955	1.73
1 T	2045	1.63
2 T	3366	1.50
3 T	4680	2.63
UNBAFFLED AND TUNED TO SPECIFIC FREQUENCY (Grid of 8*1*16)		
1 L	1966	1.94
1 T	2052	1.90
2 T	3403	2.51
3 T	4680	2.63
BAFFLED AND ORIGINAL SSME ABSORBER (Grid of 8*20*16)		
1 L	1955	1.73
1 T	1957	1.35
2 T	3023	1.08
3 T	4305	2.26

Table II illustrates how the acoustic absorber improves stability in the SSME. The original absorber design is tuned to the 3T mode and increases the combustion response of the 3T mode for neutral stability from 1.70 to 2.63 which is equivalent to going from neutral stability to a damping rate of -628 1/sec in Figure 1. This damping rate would decrease the amplitude of a 100% chamber pressure pk-pk wave to the allowable 10% amplitude in 3.6 milliseconds. The damping rate as required by ref. 28 is 18 milliseconds. Therefore, the SSME absorber design provides damping 5 times that required for the 3T mode.

The original absorber design provides a very small change in frequency and response for the 1T and 1L modes because the absorber is tuned to a much higher frequency. The 2T mode is actually made more unstable by the absorber because it reduces the frequency and decreases the chamber response. Retuning the SSME absorber to the 1T and 1L modes by decreasing the absorber opening in the chamber from 0.36 in. to 0.12 in. and increasing the aperture length from 0.5 to 1.0 inch will produce a large increase in stability, more than enough to meet the damping requirements of ref. 28. The increase in stability at the 1T and 1L frequencies is less in comparison to the stability of the original design at the 3T because the absorber open area has been reduced to obtain tuning at these lower frequencies.

Adding the baffle to the SSME changes the tuned frequencies and decreases the response required for neutral stability. The frequency change is 105 Hz for the

1T mode and 380 Hz for the 2T mode. The reduction in response is also greater for the 2T mode.

These calculations demonstrate that oscillations can occur in baffled chambers. Oscillations with either standing or spinning wave characteristics are possible. With the baffle the wave is distorted within and near the baffles, but an acoustic like wave does exist. Downstream of the baffles the wave is similar to the acoustic wave for a pure cylinder. Near the baffles they become distorted and within the baffle compartment the oscillations are predominantly axial with small variations in the radial and azimuthal directions. The decrease in response occurs because of the wave distortion produced by the baffles coupled with the steady flow profile within the chamber. The baffles reduce the loss associated with the steady flow convecting spinning oscillations out of the chamber by producing axial oscillations.

To test the capability of the FTE approach to predict observed acoustic phenomena, calculations were performed to compare with the results published by Wieber [29] and the Gemsip Program [30]. Good agreement with this data was obtained. Calculated results for the SSME were somewhat dependent on grid size, especially for the baffled chambers.[25,26]

SSME BURNING RATE OSCILLATIONS

Local burning rate oscillations resulting from the gas phase oscillations described above were calculated using the HICCIP model described in ref 24. These calculations were performed at the resonant frequency (no imaginary combustion response and no damping rate) for the SSME chamber and for the SSME with stability aids removed. The HICCIP model includes:

1. Fuel flow oscillations
2. Oxidizer flow oscillations
3. Atomization in the recess and chamber using Faeth (ref 17)
4. Vaporization using an onion skin model (ref 20).

With these models, the propellant is followed from the time it enters the fuel or oxidizer inlet dome, through the injection element, recess, and combustion chamber (as a function of time and space). Mass is always conserved throughout the combustion process. The processes are dependent on the local conditions as required by the available equations.

In order to make the burning rate oscillation calculations, a proper selection of the constants in the atomization models for the rate of atomization and drop size is required. The atomization rate constant was selected so that 50% of the oxidizer was atomized in the recess. This resulted in an atomization plane (the effective location where vaporization starts) at the injector face. The drop size constant was selected to produce a steady state gas velocity profile similar to that used in the gas phase oscillation calculations described above (99% vaporized in chamber). This resulted in a steady state drop size of 507 microns.

The oscillations in injector flow rates as given by a flow response for different rows in the injector was:

TABLE III
INJECTOR FLOW RESPONSES

Row	Fuel Response	Oxidizer Response
1	-5.9 + 1.2 * i	-0.42 - 0.30 * i
2	" "	-0.53 - 0.40 "
3	" "	-0.70 - 0.46 "
4	" "	-0.93 - 0.44 "
5	" "	-1.16 - 0.25 "
6	" "	-1.22 + 0.08 "
7	" "	-1.06 + 0.34 "
8	" "	-0.83 + 0.44 "

The large fuel response is due to the very low fuel injection pressure drop (305 psi). The variation in oxidizer response is due to the different lengths of the oxidizer tubes connecting the oxidizer manifold to the combustion chamber in the SSME injector. Oxidizer tube length varied from 5 in. near the center to 9 in. at the chamber wall.

Local combustion responses are shown in Figure 2 as a function of axial position for five different radial and tangential positions. In order to compare the local combustion rate oscillation at different locations they are nondimensionalized as follows

$$R_c = \frac{P_o \sum_t W_1 P_1}{P_{i1}^2 \sum_t W_o}$$

where

W_1 is the local oscillating burning rate
W_{o1} is the average burning rate in the first axial cell
P_o is the average chamber pressure
P_{i1} is the oscillating pressure in the first axial cell

Thus cells with very low burning rates and/or pressure amplitude do not contribute to the oscillations and are reduced proportionally in combustion response. The responses are referred to as "normalized local combustion responses" in Figure 2. This weighting eliminates large values of the combustion response at the end of the combustor where only a few drops remain to burn and the combustion response is very dependent on when in the pressure cycle these remaining drops are vaporized.

The gas oscillations and combustion response field repeat around the chamber with each baffle compartment. Therefore, only the first four tangential locations, corresponding to one baffle compartment, are shown in Fig 2 and discussed herein. Profiles inside the hub baffle (locations 2,2 4,1 and 4,4) are presented in Figure 2 as well as within a baffle compartment (locations 5,1 5,4 7,2 8,1 and 8,4).

The response for radial positions 1 through 3 (near the center and within the hub) and all tangential positions are very similar as the oscillations are spinning. These positions are represented by the response at location 2,2. Next

to the hub (radial position 4) the influence of the radial baffles outside the hub are noticed and the responses corresponding to the cells near the radial baffles (4,1 and 4,4) are shown. Within the baffle compartment the responses are given for the corners (5,1 5,4 8,1 and 8,4) and the center (7,2) to show the extreme variations noticed.

At the first axial position, the real part of the response is always a large positive number and the imaginary part is a larger negative number. This is a result of the large variation in drop size produced by the oscillation in fuel flow during a cycle. In the baffle compartments, the drop size varied between 270 and 950 microns during a cycle. With the large negative fuel response listed above the axial velocity producing atomization is very low when the pressure is high. Thus large drops are being produced when the pressure is high, resulting in low burning rates for these drops. Within the first cell 40 to 50 % of the oxidizer is burning (depending on the oscillation amplitudes). The average time for the oxidizer to travel from the injector face (atomization plane) to the center of the first axial cell is 0.40 of a cycle. Therefore, "on average" the large drops produced at the high pressure portion of the oscillations are burning at the low pressure portion of the oscillation in the first cell. This produces the large "positive" combustion response in the first cell. The fact that the combustion response has a larger negative imaginary response indicates that the time delay has resulted in the large drops burning closer to the period when the pressure is near zero and increasing.

The real part of the combustion response in the first cell varies between 1.78 (2,2 position) to 3.41 (5,4 position). The imaginary part of the combustion response varies between -5.30 (8,2 position) and -7.67 (4,1 position). These combustion responses could not be considered a constant as assumed in the simple combustion models discussed above.

The normalized combustion response drops very fast after the first cell, due to the decrease in burning rate axially and to the fact that the drops take different amounts of time to arrive at downstream cells. The effects of the variation in drop size with time are being "smeared" by the drops having different life times. It takes several cycles for the drops to arrive at these downstream cells. As a result, the contribution of the oscillating burning downstream is minimized. However, the variation in combustion response with radial and tangential directions are very large. Again, this violates the assumption used in the simple combustion models that the combustion response is uniform throughout the chamber.

To provide more detail on the variation of combustion response with radial and tangential positions, a normalized stream tube response was determined. The normalized stream tube response was calculated by summing the local combustion rates. The variation in normalized stream tube response is given in Figure 3.

Figure 3. clearly shows the large variation in combustion response with tangential position in the outer baffle compartments and with radius inside the hub compartment. The five blades of the baffle are symmetrically located around the chamber (one is at the 3 o'clock position). The combustion response is highest in the cells downstream of the baffle (at 2 o'clock) and is lowest in the cells blocking the baffle (at 12 o'clock). The highest combustion responses occur inside the hub. The phase angle of the response is indicated by a vector in Fig. 3 (zero phase angle occurs at 3 o'clock). The phase angle of the response is relatively constant in the bladed baffle compartments. A 45° phase

shift occurs between the hub compartment and the outer bladed compartments. Although the magnitude of the combustion response is highest in the hub compartment, the "poor" phase angle results in less response that is in phase with the pressure oscillation. The combustion zones in the bladed compartments are more important in driving oscillations in the SSME.

To determine the best representation of a combustion response for the entire chamber the burning rates were summed over the full chamber volume. For the baffled chamber, the "normalized full chamber combustion response" was 1.358, -2.084i. This is in contrast to the value of 1.35, +0.0i determined using the FTE approach to drive the 1T mode. Obviously, the combustion response will not drive the oscillations at the "natural frequency" since the phasing of the two vectors are not the same (the tuning frequency would be lower as indicated by Fig 1 for negative imaginary response). In addition, the local combustion oscillations calculated in the two stages are very different which means we do not have the correct oscillation profiles.

Similar local combustion response calculations were made for the unbaffled SSME with no absorber. For the 1T mode in an unbaffled chamber, all the angular positions see the same oscillation. Therefore, all the combustion responses are the same for a given radial position. The normalized stream tube combustion responses are shown in Table IV for the SSME with stability aids removed.

TABLE IV

STREAM TUBE COMBUSTION RESPONSE "Unbaffled Chamber"

	Response		Ax Pos =1	
Rad	Real	Imaginary	Real	Imaginary
1	0.784	-2.574	1.673	-3.951
2	0.294	-3.235	0.866	-5.606
3	0.787	-3.119	1.682	-5.807
4	1.139	-2.909	2.240	-5.522
5	1.302	-2.655	2.567	-5.045
6	1.336	-2.455	2.736	-4.738
7	1.329	-2.303	2.807	-4.593
8	1.346	-2.192	2.891	-4.575

Normalized Full Chamber Combustion Response = 1.272, -2.453i

Table IV again shows the large variation in combustion response with position with an unbaffled chamber. Since the wave is spinning, there are variations in only the radial and axial directions. The first axial position again has a very large value (twice the normalized stream tube value) and then rapidly drops, as seen in Fig. 2 for the baffled chamber. The largest response values are at the outside of the chamber where they are most effective in driving an oscillation. The calculated response for the full chamber has a slightly lower real value for the unbaffled chamber compared to the baffled chamber. Normally, this would indicate that the unbaffled chamber is "more stable" than the baffled chamber. With the SSME, the large combustion response is due to the varying atomization produced by the large injector fuel flow response.

The results and discussions above indicated that the fuel response is responsible for a large portion of the combustion response in the SSME. This result was checked by performing calculations with different portions of the

combustion model turned off. Calculations were also performed with different oscillations amplitude levels to show the nonlinear characteristics of the combustion process. The results of these calculations are shown in Table V.

TABLE V

FACTORS INFLUENCING COMBUSTION RESPONSE

Factor	Combustion Response 5% Pk-Pk Amp		20% Pk-Pk		80% Pk-Pk	
	Real	Imag	Real	Imag	Real	Imag
Fuel Flow Osc	1.453	-3.505	0.803	-2.268	0.166	-0.909
Axial Vel. Osc	0.025	0.652	0.025	0.655	0.020	0.424
Den. Osc	0.419	-0.046	0.417	-0.069	0.405	-0.085
Ox Flow Osc	0.242	-0.322	0.277	-0.341	0.417	-0.232
Pres. Osc	0.070	0.010	0.064	0.011	0.045	0.000
Vr & Va Osc	0.000	0.000	0.001	-0.001	-0.008	-0.002
Sum of All	(2.209)	(-3.201)	(1.414)	(-2.044)	(1.045)	(-0.804)
All Osc	2.223	-3.026	1.358	-2.084	0.646	-1.287

Table V confirms the importance of fuel flow oscillations on the combustion response. It is the phenomena making the largest contribution to combustion response at all amplitudes. The influence is very nonlinear, decreasing with increasing amplitude. At higher oscillation amplitudes the velocity of the fuel in the injector element reaches sonic velocity during a portion of the oscillation. Since the velocity cannot exceed sonic velocity, this reduces the fuel flow oscillation. To account for this fact, the fuel response in HICCIP is decreased by the square root of the oscillation amplitude at which sonic is first achieved divided by the actual amplitude. For the 20% pk-pk chamber pressure oscillations, sonic is reached in the four rows within the baffle compartment and the response is reduced to 0.8 of its value at low amplitude. At 80% Pc pk-pk, rows 2 through 10 reach sonic and the fuel response in the baffle compartment area is reduced to 0.4 of its value at low amplitude (values in Table III). As a result of this feature, the contribution of the fuel flow response decreases with increasing amplitude. The other terms are relatively insensitive to the oscillation amplitude at low amplitudes but do change at very high amplitudes.

Axial velocity oscillations are the next most important influence on combustion response after the fuel response. With the presence of the baffles, an axial wave is present in the baffle compartments, thereby producing large axial velocity oscillations. With a steady axial velocity in all cells, the axial velocity produces a sinusoidal oscillation in burning rate (the burning is Reynolds Number dependent). The baffles also reduce the frequency of the oscillation. Within the hub, the reduced frequency combined with the smaller diameter results in a large amplitude increase as you move from the injector to the tips of the baffle. This is accompanied by large axial velocity oscillations within the hub. The contribution of the axial velocity is out of phase (imaginary response) as the axial velocity oscillations are generally 120 degrees out of phase with the pressure.

Density oscillations always produce a 0.4 contribution to the combustion response. This is associated with the density term in the Reynolds number which

influences the burning rate in proportion to the square root of the Nusselt number. Since density is proportional to pressure divided by gamma, the predicted influence of density on response is about 0.4 and is independent of amplitude, frequency, drops size, etc.

Oxidizer flow oscillations have a nominal influence on the combustion response in the SSME. Oxidizer injector pressure drop is not excessive and as Table II shows the oxidizer flow response is as large as -1.2 at some rows. The negative flow response results in a positive combustion response because the time lag between injecting the oxidizer and burning is close to a half cycle. The oxidizer flow response is reduced due to the "smearing" of the flow oscillations through many cycles in the combustion process. The influence of the oxidizer flow oscillations increases with amplitude due to the change in drop size and velocity, which changes the time lag between injection and burning as well as the burning rates.

Radial and tangential gas velocity and pressure oscillations have little influence on the combustion response. Without steady state or time averaged radial and tangential velocities, the effect of these oscillations on burning rate cancel (burning rate is a function of the magnitude of velocity). The radial and tangential gas velocities would contribute to the harmonic terms in the Fourier expansion. The pressure oscillation also has little influence as it changes the "surface" temperature of the drop which slightly changes the heat required to vaporize the drop. Pressure also slightly influenced the drop size and atomization rate via the density influence in the atomization process which was considered as a pressure oscillation influence. These factors were all small and not very dependent on oscillation amplitude.

Contributions of the various factors toward the total combustion response is additive at the lower amplitudes. The term "Sum of All" in Table V is the value obtained by adding all the individual contributions. At the 5 and 20 % Pk-Pk levels, the actual calculated response using all the terms is within 5% of the individual sums. At higher amplitudes, the factors interact, as one would expect, and the sum appears to be quite different than the actual. The major influence however has been to change the phasing of the combustion response (larger imaginary and lower real values actually). Basically, this means that the time lag has changed.

All of the results presented above are very dependent on the constants used in the atomization process to determine drop size and atomization rates. These will change the steady state or time averaged profiles as well as the time lags between injection and burning. To show this influence, calculations were made with the same gas phase oscillations but with different atomization constants. These results are shown in Table VI.

TABLE VI

INFLUENCE OF ATOMIZATION CONSTANT ON COMBUSTION RESPONSE

CONSTANTS		DrSz	50%	Combustion Response Baffled		Unbaffled	
Size	Rate	Micron	Vap	Real	Imag	Real	Imag
18800	0.2666	268	0.4	0.46	-4.70	0.21	-4.74
26320	"	375	0.5	1.11	-3.29	0.96	-3.60
37600	"	507	0.9	1.36	-2.08	1.27	-2.45
52640	"	711	1.6	1.43	-1.00	1.40	-1.59
75200	"	1072	2.8	1.21	-0.06	1.18	-0.79
37600	0.1333	1558	5.7	2.59	-1.30	2.63	-1.30
"	0.1866	712	1.5	1.52	-2.15	1.36	-2.83
"	0.2666	507	0.9	1.36	-2.08	0.96	-2.45
"	0.5333	480	0.8	1.39	-1.84	1.43	-2.07

Table VI shows the strong "tuning" influence of the atomization constants. Both the size and rate constants show "optimum" values at which the response is either a maximum or minimum. The size constant of 37,600 (used in all the calculations presented above) results in a response for both the baffled and unbaffled chamber that is almost a maximum. Increasing or decreasing the size would improve stability. The rate constant of 0.2666 (also used above) results in a "minimum" response for both the baffled and unbaffled chamber. Drop size and location of the zone where 50% of the oxidizer is vaporized is also shown. Changing the rate constant changes the atomization plane and the drop size. The change in drop size is due to a change in the gas velocity field surrounding the liquid when the atomization rate is changed.

Table VI also shows the importance of the atomization constants in comparing the stability of the baffled vs unbaffled chamber. With either larger or smaller rate constants the baffled chamber is more stable than the unbaffled. At the rate constant used in the previous results, the unbaffled chamber is more stable than the unbaffled. At smaller size constants, the unbaffled chamber becomes much more stable than the baffled.

COMPUTATION TIMES

The gas oscillation and HICCIP vaporization models have been used to determine the computer time required for different grid sizes. An example of the computation time using a PC with an 80486 (33MHz) cpu to determine a solution for the gas oscillations with a specified oscillating burning rate and the combustion response with a specified gas oscillation is shown in Table VII.

TABLE VII
COMPUTATION TIME FOR SINGLE SOLUTION - 1 T MODE
486 Computer 33Mhz

Cell Size			Model	Computer Time	
Ni	Nj	Nk		Gas Oscillations	Comb Response
1	1	16	Cylinder	0.05 Min	0.04 Min
4	1	8	"	0.07 "	0.15 "
8	1	16	"	2.30 "	0.3 "
16	1	32	"	18.19 "	1.2 "
4	10	8	Baffled	0.03 Hrs	3 "
8	20	16	"	1.62 Hrs	12 "
8	20	32	"	8.03 Hrs	12 "

These results indicate that the computer time for a reasonable representation of a baffled chamber (8 radial cells, 20 tangential and 32 axial) is not excessive. The time to calculate the combustion response is much less than required to determine the gas oscillations. For a simple 1-D chamber (1x1x16), the gas oscillations require the same amount of time as the combustion response calculations. The time for gas oscillations varies with the 1.5 power of grid size while the combustion response time varies directly with the radial and tangential grid size. The effective axial grid size for the combustion response is always much finer than used in the gas oscillations program and is determined by the frequency and distance required to vaporize each drop size.

After a computation to determine the flow oscillations with a specified oscillating burning rate and a burning rate oscillation with that flow oscillation you find that the burning rate is not consistent with oscillations as one would expect from physical models. Therefore, the process has to be repeated several times (3 to 10 depending on the initial guess) before the burning rate agrees with the oscillations. Typical computational times for completing this type of calculation to determine the combustion response at a given frequency (equivalent to determining the complex frequency with a given combustion model) is:

TABLE VIII

COMPUTATION TIME FOR RESPONSE (FREQUENCY) SOLUTION
Baffled Chamber 1T Mode

Cell Size			COMPUTER TYPE		
Ni	Nj	Nk	486 (33Mhz)	VAX	Cray
4	10	8	6.6 Min	1.2 Min	
8	20	16	3.19 Hrs	36 Min	1.55 Min
8	20	32	13.7 Hrs	1.3 Hrs	3.47 Min

Computation time is dependent on the initial guess for the burning rate oscillations. If a very poor guess is used many more iterations are required before the burning rate oscillations agree with the calculated pressure profile and constant combustion response assumption. If a frequency scan is used and the solution from the last frequency is used as the next assumption, the above computer times can be decreased by as much as a factor of 4 (four). Similarly higher order modes and/or frequencies require significantly less computation time (as much as 1/3 for the 3T mode). Computer times are smaller when the original guess for the pressure and velocity perturbations in the Conjugate

Gradient Solver are zero. A good initial guess for the burning rate oscillation is important.

SUMMARY

A brief review of instability modeling prior to 1972 was made. Current approaches to instability modeling were outlined and the advantages and disadvantages of each approach were discussed. The theory for the Fourier time expansion approach was outlined in detail. Calculations were made for the combustion response profiles in the SSME combustor (with a five bladed hub baffle and absorbers). The contributions of various physical phenomena (atomization,injection, etc.) to the combustion response profiles were assessed. Computational requirements for the Fourier time expansion were discussed.

REFERENCES

1. Harrje, D.T., Reardon, F.H.: Liquid Propellant Rocket Combustion Instability, NASA SP-194, 1972.

2. Lawhead, R.B.: Photograhpic Studies of Combustion Processes in Liquid Propellant Rockets, Eigth Symposium on Combustion, The Combustion Institute, 1962.

3. Heidmann, M.F.: Visualization Studies of Combustion Instability in a Hydrogen-Oxygen Model Combustor, NASA Lewis Research Center, Film C-226.

4. Burrows, M.C.: Thermal Radiation as a Tool in Analyzing Unstable Combustion, First ICRPG Combustion Instability Conference, CPIA Pub. No 68, Vol 1, 1964, pp 301-309.

5. Crocco, L.; and Cheng, S.I.: Theory of Combustion Instability in Liquid Propellant Rocket Motors, AGARD Monograph No. 8, Butterworths Sci. Pub. Ltd. London, 1956.

6. Crocco, L.; Harrje, D.T.; and Sirignano, W.A.; et al.: Nonlinear Aspects of Combustion Instability in Liquid Propellant Rocket Motors, Princeton University, NASA CR 72426, June 1968.

7. Crocco, L.; and Mitchell, C.E: Nonlinear Periodic Oscillations in Rocket Motors with Distributed Combustion, Science and Technology, Vol. 1, No. 2. 1969.

8. Zinn, B.T.; and Savell, C.T.: A Theoretical Study of Three-Dimensional Combustion Instability in Liquid Rocket Motors, Twelfth Symposium (International) on Combustion, The Combustion Institute, 1969, pp 139-147.

9. Culick, F.E.C.: Stability of High Frequency Pressure Oscillations in Rocket Combustion Chambers, AIAA Journal, Vol. 1, No 5., 1963, pp. 1097-1104.

10. Priem, R.J.; and Rice, E.J.: Combustion Instability with Finite Mach Number Flow and Acoustic Liners. Twelfth Symposium (International) on Combustion, The Combustion Institute, 1969, pp 149-159.

11. Reardon, F.H.: Correlation of Sensitive-Time-Lag-Theory Combustion

Parameters with Thrust Chamber Design and Operating Variables, Fifth ICRPG Combustion Conference, CPIA Pub. No. 183, Dec. 1968, pp. 237-244

12. Heidmann, M.F.; and Wieber, P.R.: Analysis of Frequency Response Characteristics of Propellant Vaporization, NASA TN D-3749, Dec. 1966.

13. Heidmann, M.F.; and Groeneweg, J.F.: Analysis of the Dynamic Response of Liquid Jet Atomization to Acoustic Oscillations, NASA TN D-5339, July 1969.

14. Priem, R.J.; and Guentert, D.C.: Combustion Instability Limits Determined by a Nonlinear Theory and a One-Dimensional Model, NASA TN D-1409, Oct. 1962.

15. Hoffman, R.J.: Beltran, M.R.: Breen, B.P.; and Wright, R.O.: Extension of the Priem-Guentert Annular Combustion Instability Model to a Bi-Propellant System, Third ICRPG Combustion Conference, CPIA Pub. No. 138, Vol. I, Feb. 1967, p 309.

16. Burstein, S.Z.; and Chinitz, W.: Nonlinear Combustion Instability in Liquid-Propellant Rocket Motors. Quarterly Reports to JPL, Contract NAS7-100, Mathematical Applications Group, White Plains, New York, 1967-1968.

17. Wu, P.-K., Ruff, G.A., and Faeth, G.M., Primary Breakup in Liquid/Gas Mixing Layers, AIAA Paper 91-0285, 29th Aerospace Sciences Mtg., Jan 7-10, 1991.

18. Wu, P.-K, Tseng, L.-K., and Faeth, G.M., Primary Breakup in Gas/Liquid Mixing Layers for Turbulent Liquids, AIAA Paper 92-0462, 30th Aerospace Sciences Mtg., Jan 6-9, 1992.

19. Giridharan, M.G.: A Computer Model for Liquid Jet Atomization in Rocket Thrust Chambers, NAS8-38425.

20. Priem, R.J.: Calculating Vaporization Rates in Liquid Rocket Engines Above Critical Pressure-Temperature Conditions, 27th JANNAF Combustion Subcommittee Meeting, Nov. 1991.

21. Merkle, C.L.: Application of Computational Fluid Dynamics (CFD) Techniques to Engine Instability Study, First International Symposium on Liquid Rocket Combustion Instability, The Pennsylvania State University, Jan 18-20 1993.

22. Yang, H.Q.; et al.:Advanced CFD Methodology for Fast Transients Encountered in Nonlinear Combustion Instability Problems, NAS8-38489, July 1992.

23. Habiballah, M.; and Dubois, I.: Numerical Analysis of Engine Instability, First International Symposium on Liquid Rocket Combustion Instability, The Pennsylvania State University, Jan 18-20 1993.

24. Priem, R.J.; and Breisacher, K.J.: High Frequency Injection Coupled Combustion Instability Program (HICCIP) Status and Plans, 1990 Conference on Advanced Earth-To-Orbit Propulsion Technology, Marshall Space Flight Center.

25. Priem, R.J.; and Breisacher, K.J.: 3D Combustor Acoustic Analysis, 1992 Conference on Advanced Earth-To-Orbit Propulsion Technology, Marshall Space Flight Center.

26. Priem, R.J.; and Breisacher, K.J.: 3D Rocket Combustor Acoustics Model, AIAA-92-3228, 28th Joint Propulsion Conference, 1992.

27. Maslen, S. and Moore, F.K.: On Strong Transverse Waves Without Shocks in a Circular Cylinder, J. Aeron. Sci. 23, 583 ,1956.

28. Annom, Guidelines for Combustion Stability Specifications and Verification Procedures for Liquid Propellant Rocket Engines, CPIA Publication 247, October 1973.

29. Wieber, P.R.: Acoustic Decay Coefficients of Simulated Rocket Combustors, NASA TN D-3425.

30. Gemini Stability Improvement Program Final Report, Vol. 5, Aerojet General, August, 1965.

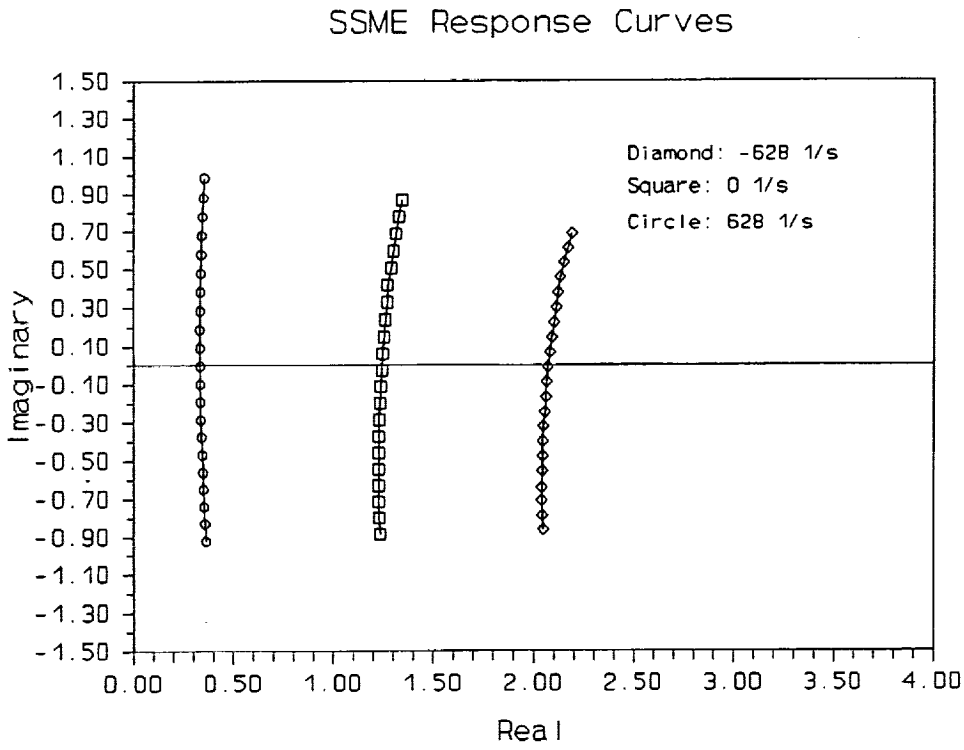
SSME Response Curves
Diamond: -628 1/s
Square: 0 1/s
Circle: 628 1/s
Imaginary
Real
1.50
1.30
1.10
0.90
0.70
0.50
0.30
0.10
-0.10
-0.30
-0.50
-0.70
-0.90
-1.10
-1.30
-1.50
0.00
0.50
1.00
1.50
2.00
2.50
3.00
3.50
4.00

Figure 1

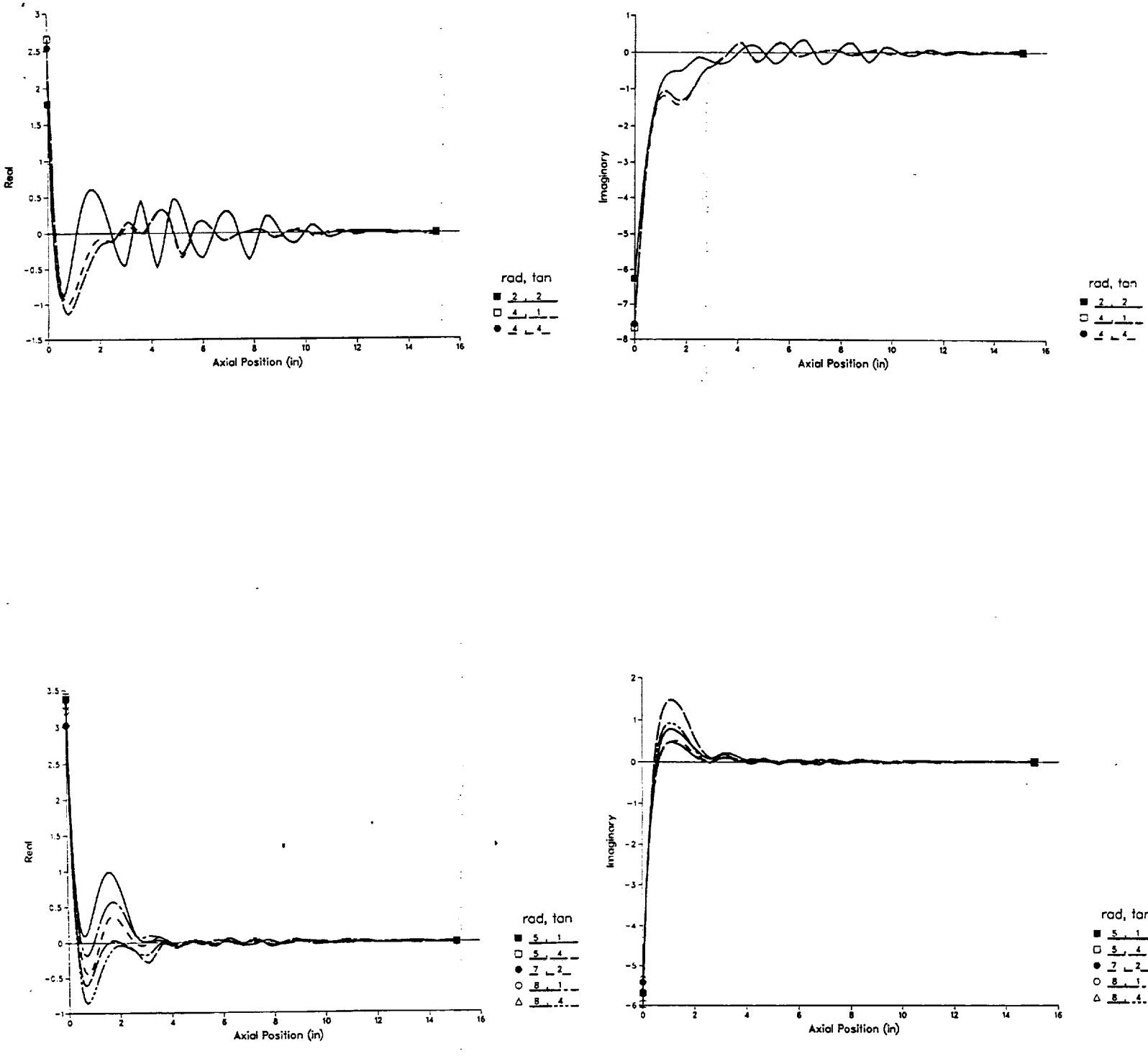

Figure 2. - Normalized local combustion responses at various radial and tangential grid positions (8 radial x 20 tangential x 30 axial cells)

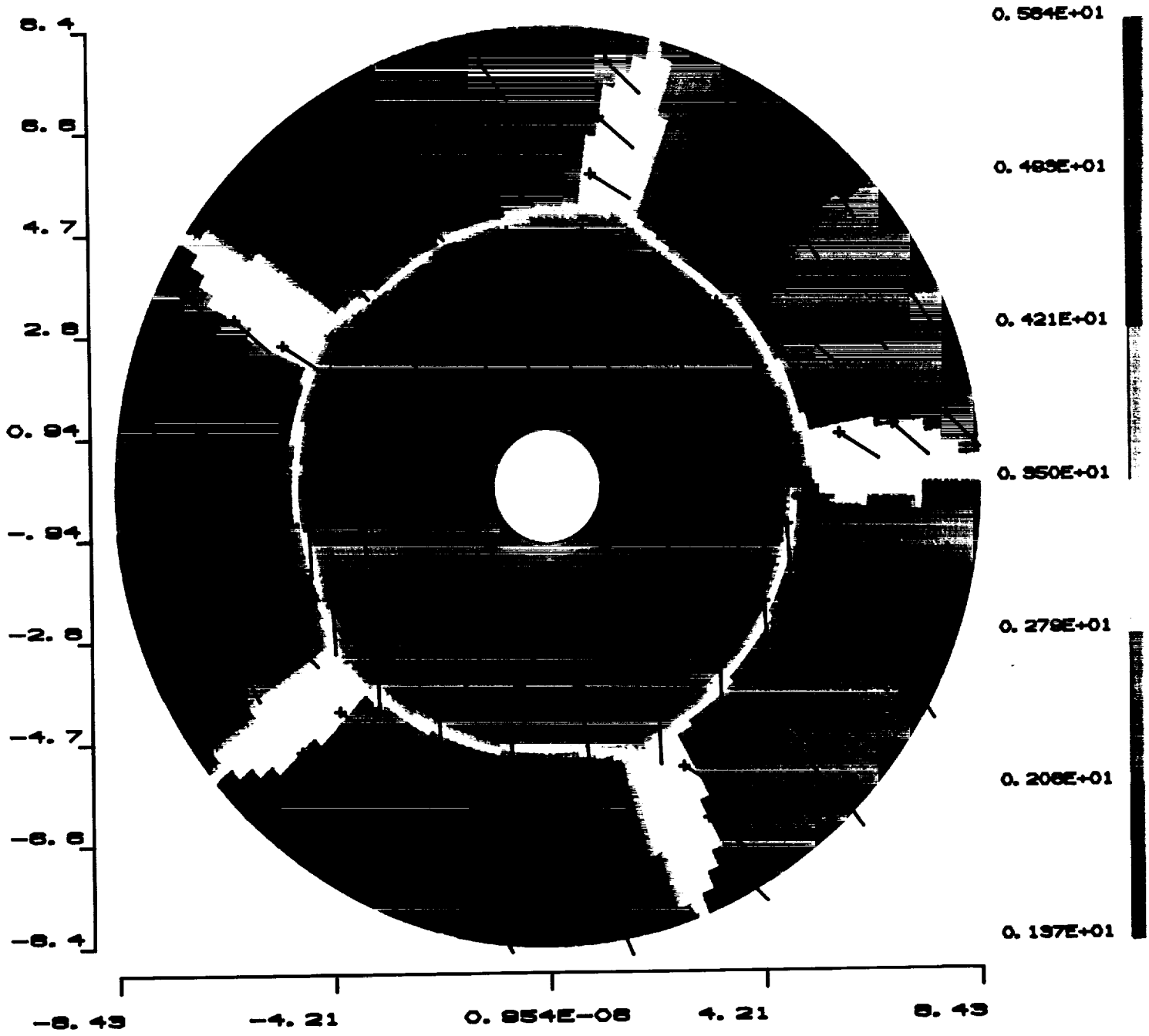

Figure 3. - Normalized stream tube responses for a baffled chamber

PRECEDING PAGE BLANK NOT FILMED

REPORT DOCUMENTATION PAGE

Form Approved
OMB No. 0704-0188

1. AGENCY USE ONLY (*Leave blank*)	2. REPORT DATE	3. REPORT TYPE AND DATES COVERED
	April 1993	Technical Memorandum

4. TITLE AND SUBTITLE

Calculations of Combustion Response Profiles and Oscillations

5. FUNDING NUMBERS

WU–590–21–11

6. AUTHOR(S)

Richard J. Priem and Kevin J. Breisacher

7. PERFORMING ORGANIZATION NAME(S) AND ADDRESS(ES)

National Aeronautics and Space Administration
Lewis Research Center
Cleveland, Ohio 44135–3191

8. PERFORMING ORGANIZATION REPORT NUMBER

E–7775

9. SPONSORING/MONITORING AGENCY NAME(S) AND ADDRESS(ES)

National Aeronautics and Space Administration
Washington, D.C. 20546–0001

10. SPONSORING/MONITORING AGENCY REPORT NUMBER

NASA TM–106135

11. SUPPLEMENTARY NOTES

Prepared for the First International Symposium on Liquid Rocket Combustion Instability sponsored by Pennsylvania State University, University Park, Pennsylvania 16802. Richard J. Priem, Priem Consultants Inc., Cleveland, Ohio and Kevin J. Breisacher, NASA Lewis Research Center. Responsible person, Kevin J. Breisacher, (216) 977–7475.

12a. DISTRIBUTION/AVAILABILITY STATEMENT

Unclassified - Unlimited
Subject Category 20

12b. DISTRIBUTION CODE

13. ABSTRACT (*Maximum 200 words*)

The theory and procedures for determining the characteristics of pressure oscillations in rocket engines with prescribed burning rate oscillations are presented. Pressure and velocity oscillations calculated using this procedure are presented for the SSME to show the influence of baffles and absorbers on the burning rate oscillations required to achieve neutral stability. Results of calculations to determine local combustion responses using detailed physical models for injection, atomization, and vaporization with gas phase oscillations in baffled and unbaffled SSME combustors are presented. The contributions of the various physical phenomena occurring in a combustor to oscillations in combustion response have been determined.

14. SUBJECT TERMS

Combustion instability; Computer models

15. NUMBER OF PAGES

30

16. PRICE CODE

A03

17. SECURITY CLASSIFICATION OF REPORT	18. SECURITY CLASSIFICATION OF THIS PAGE	19. SECURITY CLASSIFICATION OF ABSTRACT	20. LIMITATION OF ABSTRACT
Unclassified	Unclassified	Unclassified	